ISPRS Journal of Photogrammetry and Remote Sensing 66 (2011) 894–906

Contents lists available at SciVerse ScienceDirect

ISPRS Journal of Photogrammetry and Remote Sensing

journal homepage: www.elsevier.com/locate/isprsjprs

Mapping grassland leaf area index with airborne hyperspectral imagery: A comparison study of statistical approaches and inversion of radiative transfer models

Roshanak Darvishzadeh [a,*], Clement Atzberger [b], Andrew Skidmore [c], Martin Schlerf [c]

[a] Department of Remote Sensing and GIS, Faculty of Earth Sciences, Shahid Beheshti University, Tehran, Iran
[b] University of Natural Resources and Life Sciences, Vienna, Institute of Surveying, Remote Sensing and Land Information, Peter Jordan-Strasse 82, 1190 Vienna, Austria
[c] University of Twente, faculty of Geo-information Science and Earth Observation (ITC), Hengelosestraat 99, 7514 AE Enschede, The Netherlands

ARTICLE INFO

Article history:
Received 5 February 2011
Received in revised form 4 September 2011
Accepted 20 September 2011
Available online 28 October 2011

Keywords:
Mediterranean grassland
Mapping LAI
Hyperspectral
Modeling
Partial least square regression
Vegetation indices

ABSTRACT

Statistical and physical models have seldom been compared in studying grasslands. In this paper, both modeling approaches are investigated for mapping leaf area index (LAI) in a Mediterranean grassland (Majella National Park, Italy) using HyMap airborne hyperspectral images. We compared inversion of the PROSAIL radiative transfer model with narrow band vegetation indices (NDVI-like and SAVI2-like) and partial least squares regression (PLS). To assess the performance of the investigated models, the normalized RMSE (nRMSE) and R^2 between *in situ* measurements of leaf area index and estimated parameter values are reported. The results of the study demonstrate that LAI can be estimated through PROSAIL inversion with accuracies comparable to those of statistical approaches (R^2 = 0.89, nRMSE = 0.22). The accuracy of the radiative transfer model inversion was further increased by using only a spectral subset of the data (R^2 = 0.91, nRMSE = 0.18). For the feature selection wavebands not well simulated by PROSAIL were sequentially discarded until all bands fulfilled the imposed accuracy requirements.

1. Introduction

Hyperspectral remote sensing measurements have enhanced the estimation of vegetation biophysical characteristics such as leaf area index (LAI) (Lee et al., 2004; Schlerf et al., 2005; Schaepman et al., 2009). LAI, defined as one-sided leaf area divided by unit of horizontal surface area, is a key structural characteristic of vegetation because of the role of green leaves in controlling many biological and physical processes in plant canopies (Hansen and Schjoerring, 2003; Bacour et al., 2006). For example, the mapping and monitoring of LAI is mandatory for spatially distributed modeling of surface energy balance, vegetation productivity, water and CO_2 exchange (Turner et al., 1999; Pu et al., 2003).

In general, there are two common approaches to estimating vegetation biophysical characteristics from remotely sensed data (Liang, 2004; Baret and Buis, 2008). The statistical approach consists mainly in the computation of spectral vegetation indices or the use of several spectral bands in multiple (linear) regression models (e.g., Darvishzadeh et al., 2008b; Atzberger et al., 2010). To this category also belong methods based on the analysis of the red edge inflection point (Cho and Skidmore 2006); Cho et al., 2008; Darvishzadeh et al., 2009; Haboudane et al. 2008; le Maire et al. 2008), the use of artificial neural networks (Mutanga and Skidmore, 2004) and the use of spectral transformations such as band depth analysis (Schlerf et al., 2010). The physical approach involves radiative transfer models (RTM) that describe, based on physical laws, the spectral/directional variation of canopy reflectance as a function of canopy, leaf and soil background characteristics (Goel, 1989; Baret and Buis, 2008; Atzberger, 2010). Both approaches have advantages and disadvantages. While statistical approaches are fast and easy to implement, the derived relationships are recognized as being sensor-specific and dependent on site and sampling conditions, and are expected to change in space and time (Baret and Guyot, 1991; Colombo et al., 2003). Conversely, modelling the transfer and interaction of radiation inside the canopy, offers an explicit connection between the vegetation biophysical and biochemical variables and the canopy reflectance (Houborg et al., 2007). A drawback in using physically based models is the ill-posed nature of model inversion (Combal et al., 2002; Atzberger, 2004; Houborg et al., 2009), meaning that the inverse solution is not always unique as various combinations of canopy parameters may yield almost similar spectra (Weiss and Baret, 1999). The task is further complicated by the fact that radiative transfer models usually require the specification of additional input variables (e.g., soil background reflectance) for successful inversion.

* Corresponding author.
E-mail addresses: darvish@itc.nl, r_darvish@sbu.ac.ir (R. Darvishzadeh).

0924-2716/$ - see front matter © 2011 International Society for Photogrammetry and Remote Sensing, Inc. (ISPRS) Published by Elsevier B.V. All rights reserved.
doi:10.1016/j.isprsjprs.2011.09.013

Many efforts to remotely estimate and quantify vegetation properties using either statistical or physically based approaches have been carried out in the last decades. Many of the previous studies, however, investigated homogeneous and monospecific vegetation, for example, agricultural crops (Baret et al., 1987; Colombo et al., 2003; Danson et al., 2003; Atzberger, 2010), forests (Chen et al., 1997; White et al., 1997; Zarco-Tejada et al., 2004; Disney et al., 2006; Schlerf and Atzberger, 2006), or they were based on simulated data (Broge and Leblanc, 2001; Chaurasia and Dadhwal, 2004). Several studies focused on hyperspectral analysis in mixed forest stands and savanna (Wessman et al., 1988; Bateson et al., 2000; Fava et al., 2009).

Mediterranean grasslands are characterized by heterogeneous canopies with a combination of different plant species in varying proportions. This poses challenges for remote sensing applications (Fisher, 1997; Röder et al., 2007). As little is known about heterogeneous (multiple species) grassland canopies (Darvishzadeh et al., 2008a; Vohland and Jarmer, 2008), more research is warranted to better understand the capabilities and limits of different retrieval algorithms.

The aim of this study is to contribute to the comparative assessment of statistical and physical based modelling by analysing the most widely used approaches. For this, LAI in a Mediterranean grassland is estimated using both statistical models and the PROSAIL radiative transfer model. The suitability of the statistical versus the radiative transfer model approach is analyzed in terms of their prediction accuracy for estimating LAI. The RTM approach also includes a simple wavelength selection procedure. The study is based on airborne HyMap hyperspectral images acquired in parallel with field reference measurements collected during a field campaign in summer 2005 in Majella National Park, Italy.

2. Material

2.1. Study area and sampling

The study site is located in Majella National Park, Italy (latitude 41°52′ to 42°14′N, longitude 13°14′ to 13°50′E). The park covers an area of 74,095 ha and extends into the southern part of Abruzzo, at a distance of 40 km from the Adriatic Sea. The region is situated in the massifs of the Apennines. The park is characterized by several mountain peaks, the highest being Mount Amaro (2794 m). Geologically, the region is made up of calcareous rocks, which date back to the Jurassic period. The flora of the park includes more than 1800 plant species, which approximately constitute one third of the entire flora in Italy (Cimini, 2005).

Abandoned agricultural areas and settlements in Majella are returning to oak (*Quercus pubescens*) woodlands at the lower altitude (400 m to 600 m) and beech (*Fagus sylvatica*) forests at higher altitudes (1200 m to 1800 m). Between these two formations is a landscape composed of shrubby bushes, patches of grass/herb vegetation, and bare rock outcrops. The dominant grass and herb species include *Brachypodium genuense, Briza media, Bromus erectus, Festuca* sp., *Helichrysum italicum, Galium verum, Trifolium pratense, Plantago lanceolata, Sanguisorba officinalis* and *Ononis spinosa* (Cho, 2007).

A field campaign was carried out in July 2005 in which *in situ* vegetation parameters were collected. Stratified random sampling with clustering was adopted for the field data collection. For this purpose, the area was stratified into grassland, forest, shrubland and bare rock outcrops using a land cover map provided by the management of Majella National Park. Coordinates (x, y) were randomly generated in the grassland stratum to select plots. A total of 45 plots of 30 m by 30 m were generated and a GPS was used to locate them in the field. Due to logistical constraints, available man power and also the time constrain that existed in order to be parallel with the hyperspectral flight, more plots were not feasible. Care was taken to ensure sample plots were located at least 500 m (120 pixels) away from the image border. For each plot, relevant vegetation parameters were measured within four to five randomly selected subplots (1 m by 1 m) and their averages per plot were calculated. The various plots were covered with different species compositions and relative abundances, while the within-plot variability was small. The species varied in terms of leaf shape, leaf size, the number of leaves and their typical angle distribution. The within-plot variability of SPAD measurements also indicated some variation in chlorophyll contents (Darvishzadeh et al., 2008a), albeit this has not been quantified within the present study.

2.2. Field measurements

In each subplot, LAI was non-destructively measured using a widely used optical instrument, the Plant Canopy Analyzer LAI-2000 (LICOR Inc., Lincoln, NE, USA). A detailed description of this instrument is given by Li-COR (1992) and Welles and Norman (1991). Measurements were taken either under clear skies with low solar elevation (i.e., within two hours after sunrise or before sunset, respectively) or under overcast conditions. To prevent direct sunlight on the sensor, samples of below- and above-canopy radiation were made with the sun behind the operator and using a view restrictor of 45°. For each subplot, reference samples of above-canopy radiation were taken by measuring incoming radiation above the grass subplot. Next, five below-canopy samples were collected, from which the average subplot LAI was calculated.

No corrections for leaf clumping were applied as the necessary information was not available at species level. The instrument also does not distinguish between photosynthetic and non/photosynthetic components meaning that the leaf surface measured using the LAI-2000 corresponds to the plant area index (PAI) (Chen et al., 1997). Despite this fact, in the following sections, these measurements are abbreviated as LAI.

Furthermore, in each 1 m by 1 m subplot, a SPAD-502 Leaf Chlorophyll Meter (Minolta, Inc.) was used to assess leaf chlorophyll content. The between-plot variability of the leaf chlorophyll content was used as prior information to restrict the range of simulated values in the look-up table of the radiative transfer model (see 3.4). The SPAD values express the relative concentration of chlorophyll in leaves by measuring transmittance in the red (650 nm) and NIR (920 nm) wavelength regions (Minolta, 2003). SPAD measurements yield a unitless but highly reproducible measure that is well correlated with leaf chlorophyll concentration, and is commonly used to characterize chlorophyll concentration in many plant species (Campbell et al., 1990; Haboudane et al., 2002). A total of 30 leaves representing the dominant species were randomly selected in each subplot, and their SPAD readings were recorded. From the 30 individual SPAD measurements, the average was calculated. These averaged SPAD readings (unitless) were converted into leaf chlorophyll contents ($\mu g\,cm^{-2}$) by means of an empirical calibration function provided by Markwell et al. (1995) for corn and soybean. As shown in Table 1, the coefficients of variation (CV) of the measured SPAD readings were low. The low variation precluded a statistical analysis of leaf chlorophyll retrievals.

2.3. Image acquisition and pre-processing

Airborne HyMap data of the study site were acquired on 4 July 2005 during the field campaign. The flight was carried out by DLR, Germany's Aerospace Research Centre and Space Agency. The HyMap sensor contains 126 wavelengths, operating over the spectral range of 436–2485 nm. The average spectral resolution is

Table 1
Summary statistics of the measured biophysical variables of grassland sample plots (n = 41).

Measured variables	Min	Mean	Max	StDev	Range	Variation coefficient
LAI ($m^2\ m^{-2}$)	0.72	2.87	7.54	1.59	6.8	0.55
Leaf chlorophyll ($\mu g\ cm^{-2}$)	18.9	28.7	40.9	4.7	22.0	0.16
Dominant species number	1	2.34	4	0.81	3	0.35

15 nm for 436–1313 nm, 13 nm for 1409–1800 nm, and 17 nm for 1953–2485 nm. The spatial resolution of the data is 4 m (average flight height 1983 m above ground). The data were collected in four image strips with overlaps of about 30%, each covering an area of about 40 km by 2.3 km. The image acquisition was close to solar noon and the solar zenith and azimuth angles for the four image strips ranged between 30° to 33.7° and 111.5° to 121°, respectively.

The image strips were atmospherically and geometrically corrected by DLR. The atmospheric correction was performed using ATCOR4-r (rugged terrain), which is based on the MODTRAN-4 radiative transfer code. However, effects related to the sensor's large field of view in across-track direction (Schiefer et al., 2006) were not accounted for, resulting in some visible artefacts towards the borders of the strips. Conversely, our sample plots were located mainly in the central parts of the images (Fig. 1).

The geometric accuracy of the images was reported by DLR with two meters (half pixel). We also examined this accuracy by another set of images from the same area. The imagery which was taken one year before our experiment (i.e., in 2004) with the same specifications and with several control points, confirmed the specified accuracy.

The corrected strips were used to retrieve the spectra of each sample plot. Only sample plots located at least 120 pixels (500 meters) away from the border were used. As the pixel size of the imagery was 4 m, a 7 by 7 pixel window (i.e., 28 m by 28 m) centered around the central position of a plot was used for collecting grass spectra from each sample plot (plot size 30 m by 30 m). By taking only pixels located entirely in the plot, we avoided border effects. From the 7 by 7 pixel window, the average spectrum was calculated. Owing to cloud coverage in some portions of the strips, the spectra of 4 of the 45 plots could not be extracted. Hence, only the remaining 41 plots were considered for the analysis. Table 1 summarizes the statistics of the measured variables for these plots.

3. Methods

We investigated radiative transfer model inversion and two statistical modeling techniques (narrow band vegetation indices and partial least squares regression) to estimate the LAI of the studied grasslands.

3.1. Narrow band vegetation indices

Narrow band vegetation indices were computed from the extracted HyMap spectra in the form of two indices: (1) the normalized difference vegetation index (NDVI) (Rouse et al., 1974) as a representative of ratio indices (NDVI-like), and (2) the second soil-adjusted vegetation index (SAVI2) (Major et al., 1990) as a representative of soil-based indices (SAVI2-like). These two vegetation indices have been shown to perform with the highest accuracy for estimating vegetation biophysical characteristics computed from field spectra (Darvishzadeh et al., 2009).

The narrow band NDVI-like and SAVI2-like indices were systematically calculated for all possible 126 by 126 = 15,876 wavelength combinations between 436 nm and 2485 nm. The NDVI-like was computed according to:

$$NDVI_{\text{narrow}} = \frac{\rho_{\lambda 1} - \rho_{\lambda 2}}{\rho_{\lambda 1} + \rho_{\lambda 2}} \quad (1)$$

where $\rho_{\lambda 1}$ is the reflectance at wavelength λ_1 and $\rho_{\lambda 2}$ is the reflectance at wavelength λ_2 with $\lambda_1 \neq \lambda_2$.

The narrow band SAVI2-like was calculated according to the following formula:

$$SAVI2_{\text{narrow}} = \frac{\rho_{\lambda 1}}{\rho_{\lambda 2} + (b/a)} \quad (2)$$

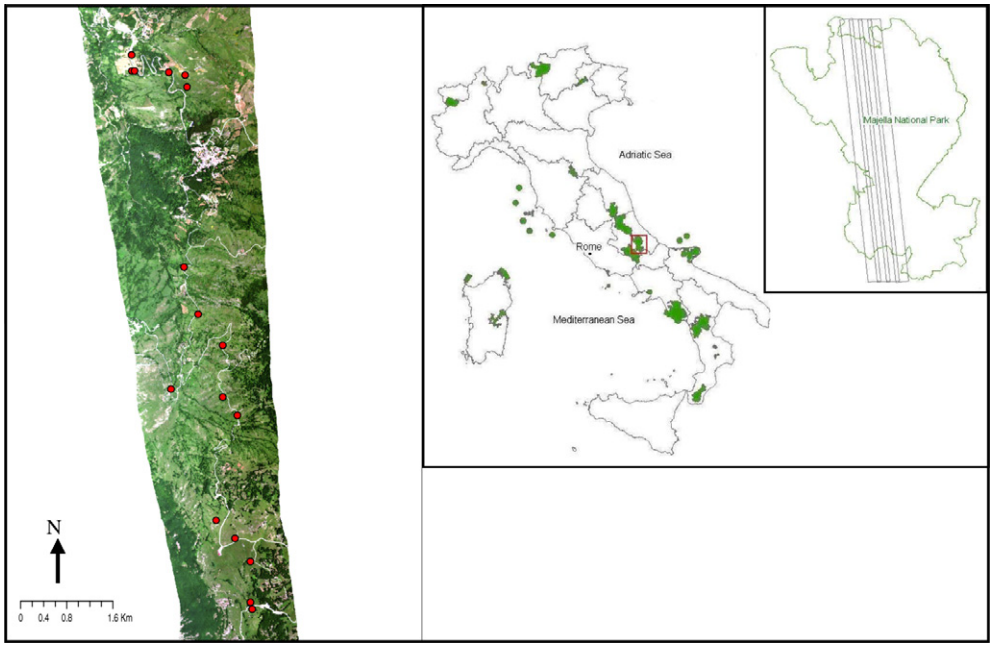

Fig. 1. True color composite of HyMap image acquired on 4 July 2005 (bands 634, 542 and 452 nm) showing part of the study area (from second image strip). The red points demonstrate the distribution of sample plots in this part of the study area. The locus map shows the flight lines of HyMap and the location of Majella National Park in Italy (red box). (For interpretation of the references to colour in this figure legend, the reader is referred to the web version of this article.)

where ρ is the reflectance, a is the slope, and b is the intercept of the soil line between bands at wavelengths λ_1 and λ_2.

The soil line parameters a and b were calculated from field spectral measurements of bare soils of a few plots with no vegetation, assuming that the measured soil optical properties were representative for the study area. For further details on procedures refer to Darvishzadeh et al. (2008a,b). We assumed that the soil line concept, originally defined for the red-NIR feature space, could be transferred to other spectral domains (Thenkabail et al., 2000; Schlerf et al., 2005) meaning that soil lines exist between all wavebands. This assumption is supported by Jacquemoud et al. (1992), who demonstrated that the soil line concept is valid for any wavelength combination, as long as the bands are not within strong water absorption bands. The soil lines are stable with changing (i) soil water content, (ii) soil roughness, and (iii) observation/illumination geometry. Consequently, the soil line parameters were systematically calculated for all possible band combinations (126 by 126) and subsequently used in Eq. (2).

3.2. Partial least squares regression

Partial least squares regression (PLSR) is a technique that reduces the large number of measured collinear spectral variables to a few non-correlated latent variables or factors while maximizing co-variability to the variable(s) of interest (Geladi and Kowalski, 1986; Hansen and Schjoerring, 2003; Cho et al., 2007; Farifteh et al., 2007). The latent variables contain the relevant information present in the measured reflectance spectra and are used to predict the dependent variable (here, LAI).

As with other linear calibration methods, in partial least squares regression the aim is to build a linear model:

$$Y = X\beta + \varepsilon \quad (3)$$

where Y is the mean-centered vector of the response variable (LAI), X is the mean-centered matrix of the predictor (spectral reflectance), β is the matrix of coefficients, and ε is the matrix of residuals. Partial least squares regression is closely related to principal component regression (Geladi and Kowalski, 1986). Whereas principal component regression performs the decomposition on the spectral data alone, partial least squares regression uses the response variable information during the decomposition process and performs the decomposition on both the spectral data and the response variable simultaneously (Schlerf et al., 2003). This explains the often better accuracy of PLS as compared to PCR in spectrometric studies (e.g. Atzberger et al., 2010). Valuable descriptions of the partial least squares regression algorithm are given in Geladi and Kowalski (1986) and Ehsani et al. (1999).

In conditions where highly correlated input variables (spectral reflectances) are included in the model, an appropriate variable selection is known to improve partial least squares regression models (Kubinyi, 1996; Davies, 2001; Cho et al., 2007). Variable selection is particularly successful if noisy wavelengths not related to the variable of interest can be eliminated. Partial least squares regression was applied to the entire reflectance spectra (436 nm to 2485 nm) and to a subset of wavelengths (see Table 2) specifically related to certain vegetation parameters (Cho et al., 2007; Darvishzadeh et al., 2008b). Regions of strong water absorption were excluded.

The optimum number of latent factors was estimated by a 'leave-one-out cross-validation' method. The number of factors that minimizes the root mean square error (RMSE) between measured and predicted values (Geladi and Kowalski, 1986) was selected. To prevent collinearity and to preserve model parsimony, the condition for adding an extra factor to the model was chosen in two ways: (i) through visual inspection of cross-validated RMSE versus the number of factors plots, and (ii) by setting the condition that adding an extra factor must reduce the $RMSE_{CV}$ by >2% (Kooistra et al., 2004; Cho et al., 2007). In addition, coefficients of determination (R^2_{CV}) between measured and predicted values in the cross-validation were used to evaluate the relationships found. The partial least squares analysis was performed using the TOMCAT toolbox 1.01 within MATLAB (Daszykowski et al., 2007).

Table 2
Subset of wavelengths for estimating grass characteristics using partial least squares regression and radiative transfer model inversion.

Wavelength nm	Vegetation parameters	Reference
466	Chlorophyll b	Curran (1989)
695	Total chlorophyll	Gitelson and Merzlyak (1997), Carter (1994)
725	Total chlorophyll, leaf mass	Horler et al. (1983)
740	Leaf mass, LAI	Horler et al. (1983)
786	Leaf mass	Guyot and Baret (1988)
845	Leaf mass, total chlorophyll	Thenkabail et al. (2004)
895	Leaf mass, LAI	Schlerf et al. (2005), Thenkabail et al. (2004)
1114	Leaf mass, LAI	Thenkabail et al. (2004)
1215	Plant moisture, cellulose, starch	Curran (1989), Thenkabail et al. (2004)
1659	Lignin, leaf mass, starch	Thenkabail et al. (2004)
2173	Protein, nitrogen	Curran (1989)
2359	Cellulose, protein, nitrogen	Curran (1989)

3.3. Validation of statistical techniques

To evaluate the performance of the statistical techniques, the cross-validation (leave-one-out) procedure was used, yielding reproducible and statistically sound results. In cross-validation, each sample is estimated by the remaining samples. This meant that for estimating LAI we developed 41 individual models, each time with data from 40 observations. The calibration model was then used to predict the observation that was left out. The resulting cross-validated RMSE ($RMSE_{cv}$) and the cross-validated coefficient of determination (R^2_{CV}) were selected as the main accuracy indicators of the statistical models in predicting unknown samples.

3.4. The PROSAIL radiative transfer model

The widely used PROSAIL radiative transfer model was selected for the physically based canopy parameter retrieval. PROSAIL is a combination of the SAIL canopy reflectance model and the PROSPECT leaf optical properties model. Both sub-models are relatively simple and need only a limited number of input parameters with reasonable computation time, which makes model inversion for retrieval of leaf and canopy parameters feasible.

The PROSPECT model (Jacquemoud and Baret, 1990; Jacquemoud et al., 1996; Fourty et al., 1996) calculates the leaf hemispherical transmittance and reflectance as a function of four input parameters: the leaf structural parameter N (unitless); the leaf chlorophyll $a+b$ concentration C_{ab} ($\mu g\ cm^{-2}$); the dry matter content C_m ($g\ cm^{-2}$); and the equivalent water thickness C_w (cm). The spectral leaf optical properties (leaf reflectance and transmittance) calculated by PROSPECT are inputs into the SAIL canopy reflectance model. This model (Verhoef, 1984; Verhoef, 1985) is a one-dimensional bidirectional turbid medium radiative transfer model that has been later modified to take into account the hot spot effect in plant canopy reflectance (Kuusk, 1991). Turbid medium defines the canopy as a horizontally homogenous and semi-infinite layer that consists of small vegetation elements that act as absorbing and scattering particles of a given geometry and density. The model has been successful when used in

homogeneous vegetation canopies (Verhoef, 1984; Meroni et al., 2004; Atzberger and Richter, 2009). Apart from the leaf reflectance and transmittance, the SAIL model requires eight input parameters to simulate the top-of-canopy bidirectional reflectance. These are sun zenith angle, t_s (deg); sensor viewing angle, t_o (deg); relative azimuth angle between sensor and sun, *phi* (deg); fraction of diffuse incoming solar radiation, *skyl*; background reflectance (soil reflectance) for each wavelength, *rsl*; *LAI* (m^2 m^{-2}); average leaf inclination angle, *ALA* (deg); and the hot spot size parameter, *hot* (m m^{-1}), defined as the ratio between the average size of the leaves and the canopy height (Verhoef, 1985). To account for soil brightness changes induced by moisture and roughness, we used a (multiplicative) soil brightness parameter, *scale* (Richter et al., 2009). Therefore, in PROSAIL 12 input parameters that characterize the leaf, the canopy and the soil have to be specified. Of the 12 input parameters, four parameters were fixed (sensor viewing angle, azimuth angle, sun zenith angle and fraction of diffuse incoming solar radiation). For the eight remaining input parameters (i.e., LAI, ALA, scale, hot, *N*, C_{ab}, C_m and C_w), 100,000 parameter sets were generated randomly (Table 3) to realize the look-up table (LUT) used for model inversion.

3.4.1. The look-up table (LUT) inversion

Look-up-tables (LUT) provide an easy way for inverting radiative transfer models (Knyazikhin et al., 1999). Compared to numerical optimization and neural network methods, LUT constitute an interesting alternative because they permit a global search (avoiding local minima) while showing less unexpected behavior when the spectral characteristics of the targets are not well represented by the modeled spectra (Atzberger, 2010). A LUT is built in advance of the actual inversion through forward calculations using the radiative transfer model. For the inversion, only search operations are needed to identify the parameter combinations that yield the best fit between measured and LUT spectra. However, to achieve high accuracy for the estimated parameters, the dimension of the table must be large enough (Weiss et al., 2000; Combal et al., 2002; Tang et al., 2006).

To build the LUT, 100,000 parameter combinations were randomly generated (uniform distributions) and used in the forward calculation of the PROSAIL model. Working with the same RTM, a size of 100,000 LUT entries was found by Weiss et al. (2000) and Richter et al. (2009) to be a good compromise between IT requirements and the accuracy of the estimates. We also tested normally distributed random parameters and found no significant differences (not shown). The ranges (minimum and maximum) for each of the eight "free" model parameters are reported in Table 3. To prevent too-wide parameter spaces, and to increase the sampling density, the approximate maximum and minimum values of LAI, C_{ab} and ALA (recorded along with LAI, using the LAI-2000 instrument) were selected based on prior knowledge from the field data collection (Combal et al., 2003). Concerning the leaf structural parameter *N* in PROSPECT we selected a range of 1.5 to 1.9 since grasses have relatively thin leaves. This range was used in a previous study by Darvishzadeh et al., 2008a and is in agreement with the mean value ($N = 1.6$) that Vohland and Jarmer (2008) used for grassland species, it is also a little more limited than the more general study by le Maire et al. (2004) and le Maire et al. (2008). In a direct simulation mode, Haboudane et al. (2004) and Houborg et al. (2007) used a fixed value of 1.55 for various crops, including corn, soybean, wheat and spring barley. Jacquemoud et al. (2000) used a fixed value of $N = 1.7$ for soybean, while Atzberger et al. (2003) used a range of $N = 2 \pm 0.34$ for wheat crop. The ranges of other input parameters (C_w, C_m and hot) were similarly selected (Table 3) in agreement with the existing literature (Combal et al., 2003; Haboudane et al., 2004; le Maire et al., 2004; Schlerf and Atzberger, 2006; Cho, 2007; Houborg and Boegh, 2008; le Maire et al., 2008; Haboudane et al., 2008).

To represent soil optical properties we used the measured average bare soil reflectance spectra of the study area. This step would need to be repeated when transferring the modeling approach to landscapes with strongly differing soil optical properties. The *scale* parameter range shown in Table 3 was used to mimic eventually occurring soil brightness changes (Richter et al., 2009). With respect to the fraction of diffuse incoming solar radiation (*skyl*), a fixed value of 0.1 across all wavelengths was used, as in many similar studies (Cho, 2007). Hence, we have neglected the fact that the amount of diffuse sky light depends on atmospheric conditions and solar zenith angle, and, furthermore, is wavelength-dependent. This simplification seems justified, however, by the fact that *skyl* has only a very small influence on canopy reflectance (Clevers and Verhoef, 1991) and by the lack of on-site measurements of *skyl*. Since most of the plots were located close to the nadir line of the image strips, the sensor viewing angle (t_o) and the relative azimuth angle (*phi*) were fixed at 0°. The sun zenith angle was fixed at 31.5°.

To find the solution to the inverse problem for a given canopy spectra, for each modeled reflectance spectra of the LUT the root mean square error between measured and modeled spectra ($RMSE_r$) is calculated according to:

$$\mathrm{RMSE}_r = \sqrt{\frac{\sum_{i=1}^{n} (R_{\mathrm{measured}_i} - R_{\mathrm{lut}_i})^2}{n}} \quad (4)$$

where $R_{measured}$ is the measured reflectance at wavelength λ, Rlut is the modeled reflectance at the same wavelength in the LUT, and n is the number of wavebands. Traditionally, the solution is regarded as the set of input parameters corresponding to the reflectance in the LUT which provides the smallest $RMSE_r$. However, this solution is not always the optimal solution since it may not be unique (ill-posed problem) (Atzberger, 2004). To overcome this problem and to enhance the consistency of the estimated variables, we also investigated the mean and median from the best 10 and 100 simulations, respectively (Combal et al., 2003).

An appropriate band selection – or alternatively the weighting of different spectral bands – is known to improve radiative transfer model inversion and prevents bias in the estimation of the variables of interest (Meroni et al., 2004; Schlerf and Atzberger, 2006; Lavergne et al., 2007). This is particularly the case if the hyperspectral data set contains wavebands that are either noisy or poorly modeled by the radiative transfer model being inverted.

Table 3
Specific ranges for nine input parameters used for generating the LUT, using forward calculation of the PROSAIL model. Within the specified ranges, parameter values were drawn randomly (uniform distributions).

Parameter	Abbr. in model	Unit	Minimum value	Maximum value
Leaf area index[a]	LAI	m^2 m^{-2}	0	8
Mean leaf inclination angle[a]	ALA	Deg	40	70
Leaf chlorophyll content[a]	C_{ab}	μg cm^{-2}	15	45
Leaf structural parameter	*N*	No dimension	1.5	1.9
Dry matter content	C_m	g cm^{-2}	0.005	0.010
Equivalent water thickness	C_w	cm	0.01	0.02
Hot spot size	hot	m m^{-1}	0.05	0.10
Soil brightness	scale	No dimension	0.5	1.5

[a] The minimum and maximum values are selected based on prior knowledge from field measurements.

Neither the selection of an optimal spectral subset, nor the weighting of spectral bands, are trivial problems but are still open issues within the remote sensing community (Meroni et al., 2004; Lavergne et al., 2007; Atzberger, 2010). Therefore, to account for band selection, the inversion of the model was also tested with a small number of pre-defined bands related to leaf chlorophyll, LAI and leaf dry mass (Table 2). As an alternative, we also propose a simple approach which discards wavelengths that are not well modeled by PROSAIL. The iterative approach starts with an elimination of the worst modeled spectral band (calculated across all sample plots). The LUT inversion is than repeated and the modeling accuracy of the different bands is again assessed. The process continues until all bands are modeled with accuracies better than a user-specified threshold (RMSE $\leqslant$ 0.02).

3.4.2. Evaluation of PROSAIL in forward mode

It is recommended to carefully evaluate the performance of the selected radiative transfer model in forward mode before starting the RTM inversion (Baret and Buis, 2008; Stuckens et al., 2009). For this reason, it was checked whether PROSAIL is well adapted to simulate the grassland spectra given the measured LAI and C_{ab} values. Without such a check, one would invert the radiative transfer model without being sure that it is well adapted to the canopy of interest (here Mediterranean grasslands).

To quantify the agreement between measured and simulated data, we calculated a reflectance mismatch between each HyMap spectra and the reflectances in a simulated training database. The training database was established for each plot individually, as each plot is characterized by a particular LAI and C_{ab} combination. For each plot, we took the measured LAI and C_{ab} values and the prescribed ranges of the other parameters (Table 3) and run PROSAIL in forward mode (10,000 simulations). Since LAI and C_{ab} may have had some possible measurement errors, the measured parameter values for these two variables were varied by 15 percent around their field measured mean values.

Ten wavelengths well spread over the whole range – and outside the bands that are not well simulated by PROSAIL (Darvishzadeh et al., 2008a) – were used to assess the simulation accuracy of PROSAIL in forward mode. The reflectance mismatch was then defined as the minimum RMSE calculated between the measured spectrum and the best fitting spectrum of the training database. The procedure was repeated for all 41 plots.

4. Results

4.1. Narrow band vegetation indices

Narrow band indices were calculated in the form of NDVI-like and SAVI2-like indices from the HyMap reflectance spectra, using all possible two-band combinations. The coefficients of determination (R^2) between these narrow band vegetation indices and the *in situ* LAI measurements were computed. These results are illustrated in Fig. 2 in form of a 2-D correlation plot. The meeting point of each pair of bands in a 2-D plot corresponds to the R^2 value between the LAI value and the vegetation index value calculated from the HyMap reflectance values in those two wavelengths. The 2-D correlation plots are rather different with those presented in le Maire et al. 2008. The discontinuities that are observed in these plots are due to gaps in the reflectance values that exist in the data (e.g., regions with strong water vapor absorption) whereas these regions in le Maire et al. 2008 are left blank. Moreover, in their study individual wavelengths are used for plotting the RMSE values while here the correlation (R^2) was assessed at discrete combinations of two HyMap bands, whereas for convenience we decided to label the x- and y-axis as "wavelength". Based on the R^2 values in the 2-D correlation plots, band combinations that formed the best indices were determined for LAI estimation.

The three best performing band positions are tabulated in Table 4 together with cross-validated R^2, RMSE and the normalized RMSE (nRMSE = RMSE/mean field measured LAI) statistics. The cross-validated R^2 between the grass LAI and the two narrow band indices were relatively high (0.83 to 0.85). Normalized RMSE were lower than 0.25. The narrow band SAVI2-like performed somewhat better than did the narrow band NDVI-like. This may indicate a slight advantage of the soil-based SAVI2-like index over the ratio index NDVI-like probably related to a better minimization of soil background effects.

As it is also can be observed from Table 4, for both indices, the "optimum" bands for LAI estimation were found in the NIR and SWIR regions. This confirms previous studies that have demonstrated that the bands from these regions are important for LAI estimation (Brown et al., 2000; Cohen and Goward, 2004; Lee et al., 2004). Fig. 2 (c and d) highlights regions where $R^2 \geqslant 0.8$ for LAI. The observed patterns are in agreement with a previous study by Darvishzadeh et al. (2008b), who found similar patterns for these variables when using a different sampling and sensor (field spectrometer).

Fig. 3 shows the relationships between the estimated cross-validated LAI and measured LAI when using narrow band SAVI2-like. Only a slight saturation tendency for high LAI can be observed. However, as only four out of forty-one samples had LAI > 5, the statement remains vague.

4.2. Partial least squares regression

The relationships between grass variables and reflectance spectra were modeled using partial least square regression (PLS). The optimal number of latent regression factors required to prevent over-fitting in the final model was four. Similar numbers of latent regression factors were found in analog studies (Atzberger et al., 2010). Cross-validated results using the entire reflectance spectra as inputs are shown in Fig. 4. The corresponding statistics are reported in Table 5.

Compared with narrow band vegetation indices (Table 4), PLS slightly increased the cross-validated R^2 value, but was not able to decrease the $nRMSE_{cv}$. As can be observed from the scatter plot, high LAI values were again slightly underestimated, similar to Fig. 3 where SAVI2-like has been used as a predictor. Once more, having only few sample points with high LAI values makes the estimation of the saturation asymptote difficult.

We formed a spectral subset of the full spectrum to build new PLS models by selecting a subset of wavelengths closely related to vegetation parameters (see Table 2). Waveband selection did not have any negative effect on the R^2 values and even slightly decreased the $RMSE_{cv}$ from 0.68 to 0.64. This supports the view that for vegetation studies a cautiously selected spectral subset includes almost the entire information of the full spectral resolution (Fourty and Baret, 1997). At the same time, eventually occurring problems with noisy wavebands are minimized. In our case, assuming a linear relation between LAI and the spectral variables, twelve (two) bands contained most of the LAI relevant information when used in a PLS model or combined, for example, in the form of SAVI2-like.

4.3. Inversion of PROSAIL

4.3.1. Forward modeling results

The results of the evaluation of the model in the forward mode are summarized in Fig. 5. The top figures show the frequency distribution (Fig. 5a) and empirical cumulated distribution function (Fig. 5b) of the root mean square error (RMSE) between the measured spectrum and the best fitting profile in the training database.

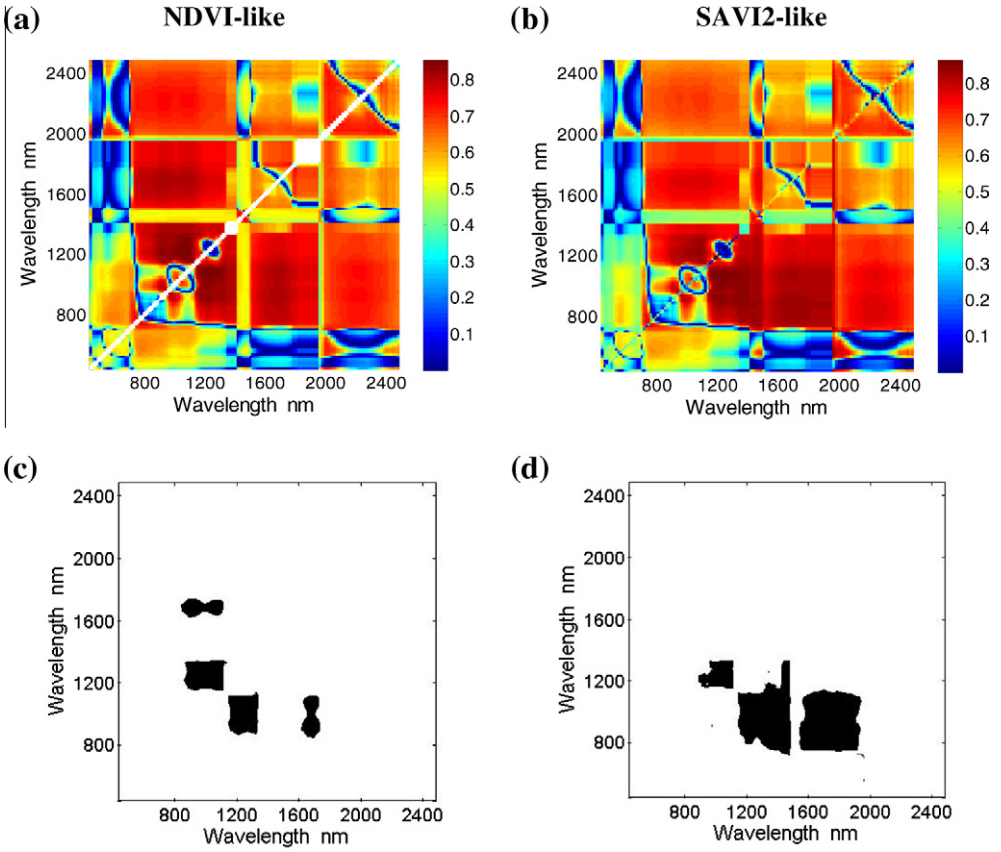

Fig. 2. 2-D correlation plots illustrating the coefficient of determination (R^2) between LAI and (a) narrow band NDVI-like (b) narrow band SAVI2-like for all possible 2-band combinations of the HyMap sensor. Please note that the discontinuities observed in the figures (especially around 1340–1400 and 1800–1950) are due to the gaps which exist in HyMap band setting. (c) and (d) highlight regions with high correlation ($R^2 \geqslant 0.8$) between LAI and narrow band vegetation indices for NDVI-like (c) and SAVI2-like (d).

Table 4
The best three band positions (derived from 2-D correlation plots) and performance of narrow band vegetation indices for predicting LAI in Majella National Park, Italy, using HyMap data. R^2_{CV} is the cross-validated coefficient of determination between estimated and predicted LAI; $RMSE_{cv}$ is the cross-validated root mean square error; and $nRMSE_{cv}$ is the normalized cross-validated root mean square error, i.e., $RMSE_{cv}$ divided by mean ($n = 41$).

	Narrow band VI	λ (nm)	R^2_{CV}	$RMSE_{cv}$	$nRMSE_{cv}$
LAI	NDVI-like	1068/1215	0.83	0.65	0.23
		1068/1229	0.83	0.66	0.23
		1053/1215	0.83	0.66	0.23
	SAVI2-like	1068/1229	0.85	0.62	0.21
		1068/1243	0.84	0.62	0.21
		1053/1229	0.84	0.63	0.22

The three best and the three worst simulated deviance spectra (measured HyMap reflectances minus the simulated reflectances of the training database in reflectance units) are shown in the lower part of the figure (Fig. 5c and d).

A perfect fit would result in horizontal lines at value zero. This is more or less the case for the three best spectra (Fig. 5c). However, for the three worst spectra significant differences between simulated and measured spectra can be observed (Fig. 5d). This shows that no combination in the LUT was representing these spectra. This could be interpreted as an incapability of the RTM to simulate the actual canopy. Possibly, the mismatch could also result from measurement errors. As most spectra were well modeled (Fig. 5a and b), and as the deviances were relatively modest even for the three worst cases, we believe that a combination of factors is responsible for the rather weak accuracy of these three spectra.

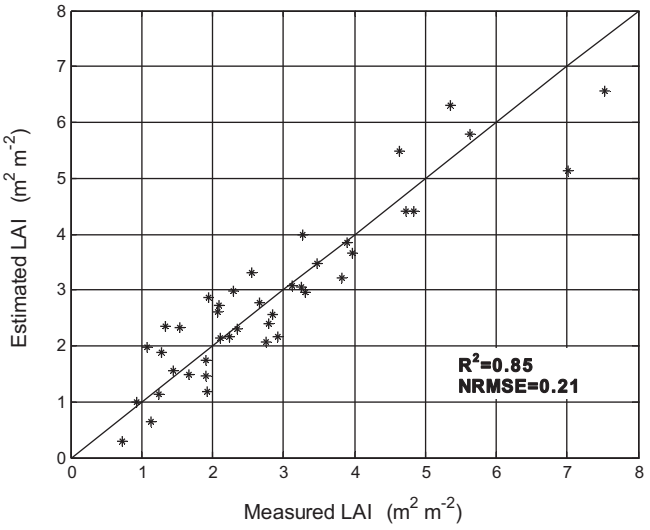

Fig. 3. Cross-validated prediction of LAI in Majella National Park, Italy, using narrow band SAVI2-like. The optimum wavebands are reported in Table 4.

In general terms, the forward modeling exercise showed that with the ground measured LAI and C_{ab} (varied by 15 percent around their recorded value) one is able to simulate the observed spectra quite accurately. We thus concluded that the selected PROSAIL radiative transfer model can be employed for analyzing our Mediterranean grassland targets.

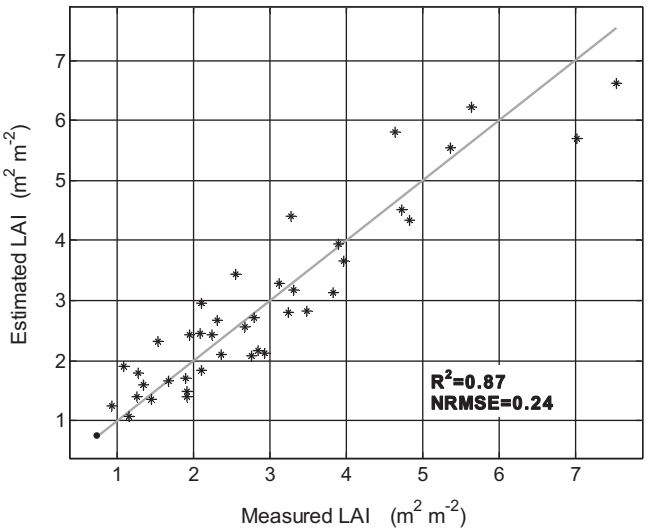

Fig. 4. Cross-validated prediction of LAI in Majella National Park, Italy, using the entire reflectance spectra of HyMap in partial least squares regression models with 4 latent factors.

Table 5
Performance of partial least squares regression for predicting LAI in Majella National Park, Italy, using HyMap data. R^2_{CV} is the cross-validated coefficient of determination between estimated and predicted LAI; $RMSE_{cv}$ is the cross-validated root mean square error; and $nRMSE_{cv}$ is the normalized cross-validated root mean square error ($n = 41$).

		No. of factors	R^2_{CV}	$RMSE_{cv}$	$nRMSE_{cv}$
Entire spectra	LAI	4	0.87	0.68	0.24
Spectral subset I (Table 2)	LAI	4	0.87	0.64	0.22

4.3.2. Inversion using the full spectral information

To find the solution to the inverse problem, the LUT was sorted according to the cost function (equation 4) and the set of variables where the cost function was minimal was considered as the solution. In the following, we will refer to this as "best-fit". Fig. 6 illustrates measured and simulated canopy reflectance spectra found in this way for two subplots with contrasting LAI values.

As can be observed from Fig. 6, the simulated reflectances were generally in relatively good agreement with the measured reflectances for canopies with different LAI values. A more concise analysis reveals that most spectral bands were modeled with average absolute error (AAE) (Eq. (5)) lower than 0.02 reflectance units (Fig. 7).

$$AAE_{\lambda} = \frac{1}{q}\left|\sum_{i=1}^{q}(R_{measured_{\lambda}} - R_{bestfit_{\lambda}})\right| \quad (5)$$

where $R_{measured}$ is the measured reflectance at wavelength λ; $R_{bestfit}$ is the best-fit reflectance at the same wavelength; and q is the number of samples (=41). In sub-section 4.3.3 we present a spectral subset where these bands (with AAE greater or equal to 0.02) have been excluded.

The relation between the measured and estimated LAI (best-fit) is demonstrated in Fig. 8. It can be observed that the PROSAIL inversion yielded similar accuracies compared to the statistical models ($R^2 = 0.86$ and nRMSE = 0.24). In contrast to the empirical models, a slight offset can be noted.

Investigation of the histograms of the remaining PROSAIL parameters (*N*, ALA, C_{ab}, C_m, C_w, *hot* and *scale*) revealed that for most of them, several (30 out of 41) sample plots reached the upper/lower boundary of at least one model parameter (not shown). This highlights the importance of using appropriate prior information when constructing LUT for radiative transfer model inversion (Combal et al., 2003). The fact that for some samples the boundaries were reached could also be the result of either noisy or poorly modeled wavelengths, in particular by considering that the parameter ranges were relatively large (Table 3) (Schlerf and Atzberger, 2006; Darvishzadeh et al., 2008a).

We also evaluated the retrieval accuracy if "multiple solutions" are used (i.e., the mean of the first 10 and the first 100 best fits of the LUT) thus minimizing the ill-posedness of the inverse problem (Combal et al., 2003). Table 6 compares the "multiple solutions" with the "best-fit" LUT solutions, demonstrating how different solutions affect the inversion results. We tested the significance of the results and found no significant differences between the statistical parameters used for any number of solutions (one-way ANOVA; $p > 0.05$). Nevertheless, throughout the rest of this study, we used the LUT inversion using the first 10 solutions for estimating the grass LAI.

4.3.3. Use of spectral subsets in the inversion process

The average absolute errors (AAE) between measured and best-fit spectra as a function of wavelengths are plotted in Fig. 7. It can be seen that the AAE in some regions is relatively high (greater than 0.02), especially close to the water vapor absorption regions (1135 nm to 1400 nm, and 1820 nm to 1940 nm). We considered bands with an AAE greater or equal to 0.02 as wavelengths being either poorly modeled or defectively measured. The aim was to use a spectral subset for PROSAIL inversion where all bands are modeled with AAE < 0.02. This was achieved using an iterative procedure starting with the full spectral resolution. In the first iteration, the band having the highest AAE was removed and the LUT inversion was repeated (as well as the AAE calculation – Eq. 5). The process was repeated until all remaining wavelengths had an AAE less than 0.02. The elimination of wavelengths stopped after 19 iterations. The remaining wavebands ($n = 107$) were termed "subset II". Subset II and the wavelengths identified from literature (Table 2) (subset I) were used for the inversion procedure.

The role of the spectral subsets in the estimation of grassland LAI was again evaluated on the basis of the R^2 and the normalized RMSE between the measured and estimated LAI. The results showed that, after removing the wavelengths not well modeled by PROSAIL (and using the 10 best fits of the LUT), the relationship between measured and estimated LAI was considerably improved (Table 7). Using subset II, LAI was estimated with an accuracy of 0.53 $m^2\ m^{-2}$, which represents 18 percent of the average field measured LAI (nRMSE) or just 8 percent of the range of field measured LAI ($0.7 \leqslant LAI \leqslant 7.5$). The positive influence of using multiple solutions for coping with the ill-posedness of the inverse problem is evident by comparing the mentioned results with those obtained using the same subset but the best fitting spectra (Table 7). On the contrary, employing subset I could not improve the retrieval accuracy compared to the full spectral resolution (Table 7). Compared to subset II, much lower accuracies have been obtained. This highlights the need for a careful elimination of wavebands not well simulated by the RTM.

4.4. Mapping grass variables

The LAI of the Majella grassland was mapped using the PROSAIL model. A grassland mask separated non-grass areas from grassland in the HyMap image strips. The mask was established using a maximum likelihood classification and eliminated areas occupied by other land cover types (mainly forest and housing). The masked HyMap image was used as input to the inversion process and a map of predicted LAI was retrieved using the spectral subset II and the mean of 10 best fitting LUT spectra. The resulting map is presented in Fig. 9. It confirms the spatial distribution of LAI with respect to the forage conditions and grazing intensities (Bemigisha, 2008). It is also closely matched with our observation during the field campaign (Cho, 2007; Bemigisha, 2008).

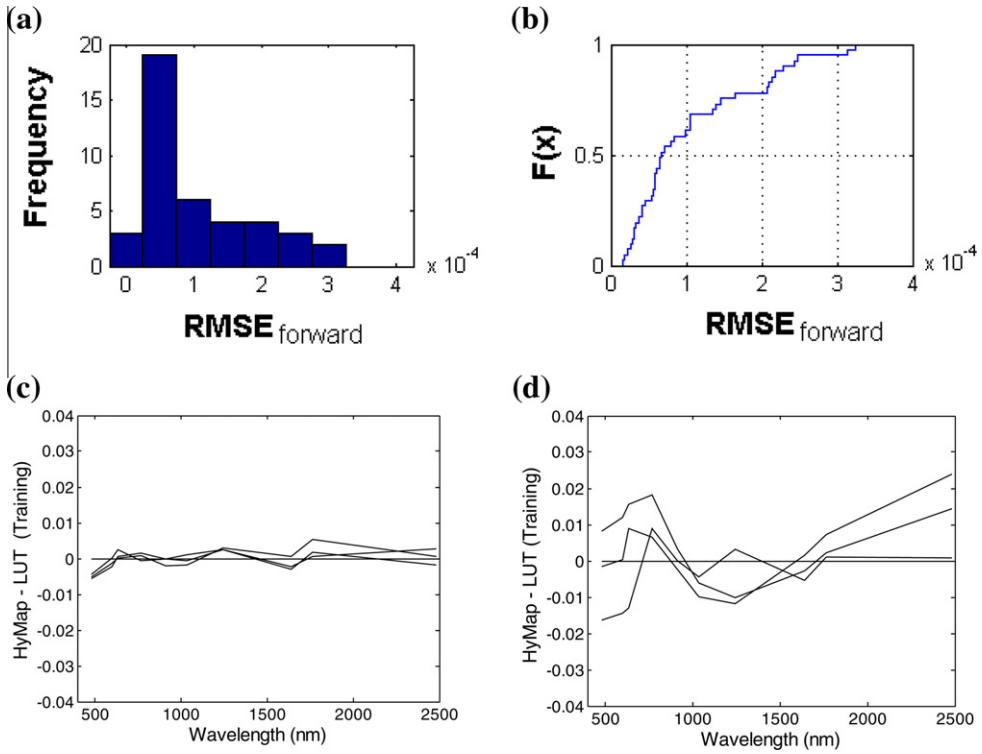

Fig. 5. Evaluation of the PROSAIL radiative transfer model in forward mode using field measured model variables as inputs. (a) Frequency distribution of the RMSE between the HyMap spectra and the best fitting spectra of the training data base. (b) Same data shown as empirical cumulated distribution function, (c) spectral deviances between HyMap spectra and the best fitting spectra of the training data base for the three best cases (d) the same for the three worst cases.

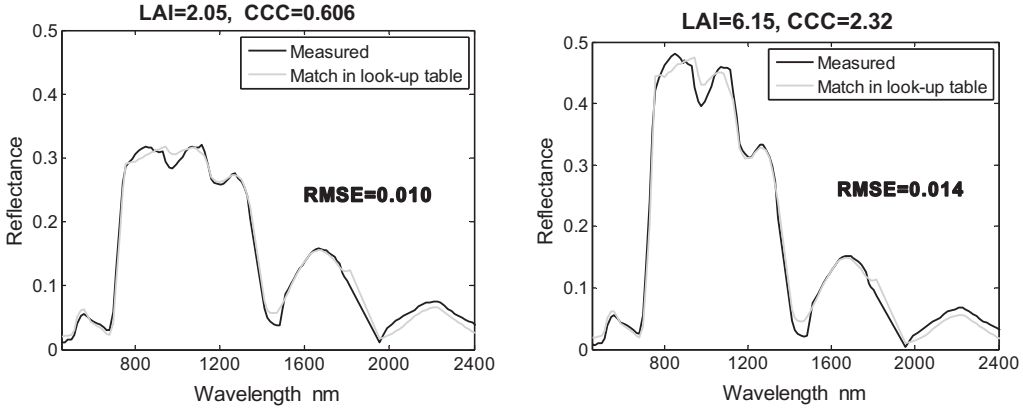

Fig. 6. Measured and PROSAIL simulated grass canopy reflectance spectra of two sample plots, with LAI equal to 2.1 (left) and 6.2 (right), respectively. Measured and simulated reflectance values are at discrete wavelengths; lines are only drawn to ease interpretation. CCC is the canopy chlorophyll content (LAI × Cab).

The mean LAI obtained for all image pixels representing grassland was 2.91 m^2 m^{-2} which is very close to the mean LAI of the samples measured during the field measurement (2.87; Table 2). As for the field samples (Table 1), most modeled LAI lay between 1 and 4.

5. Discussion

Compared with the statistical models used in this study, inversion of the radiative transfer model yielded a similar (full spectral resolution) or even higher (spectral subset II) R^2 (and lower normalized RMSE) values between field-measured and modeled LAI. This supports previous studies (Gemmell et al., 2002; Schlerf and Atzberger, 2006), which demonstrated that inversion of a radiative transfer model may yield accuracies comparable to those of statistical approaches. The main benefit of using the physical rather than the statistical approach is that comprehensive field measurements are not required for model calibration. However, inversion of the physically based models is always hampered by the ill-posed inverse problem (Combal et al., 2002; Atzberger, 2004). In the current work this problem was alleviated by using multiple solutions instead of the best fitting spectra. An additional challenge in using physical based models is the large number of input variables that must be specified as well as the computational load for inverting the radiative transfer models.

The optimum bands for use within the two vegetation indices (NDVI-like and SAVI2-like) were found in the NIR to SWIR regions. This confirms previous studies where SWIR bands significantly strengthened the relationship between the spectral reflectance and LAI (Nemani et al., 1993; Brown et al., 2000; Cohen and Goward, 2004; Lee et al., 2004).

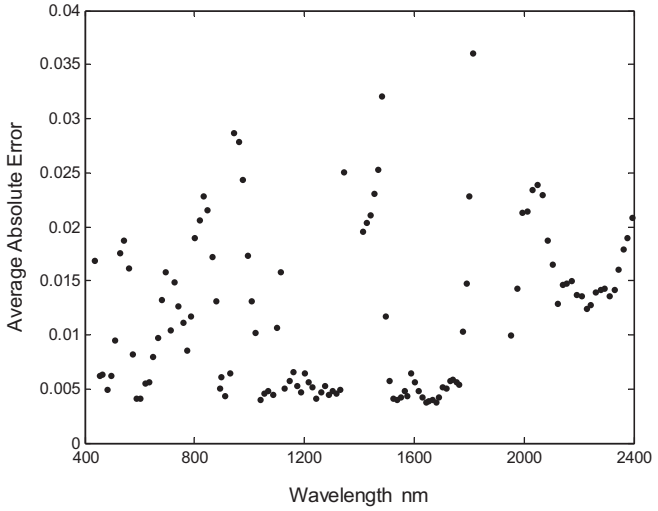

Fig. 7. Absolute average error (AAE) between best-fitting spectra in the LUT and the measured HyMap reflectance spectra as a function of wavelength. The AAE has been calculated between the measured HyMap and the best fitting LUT spectra of 41 sample plots (Eq. 5).

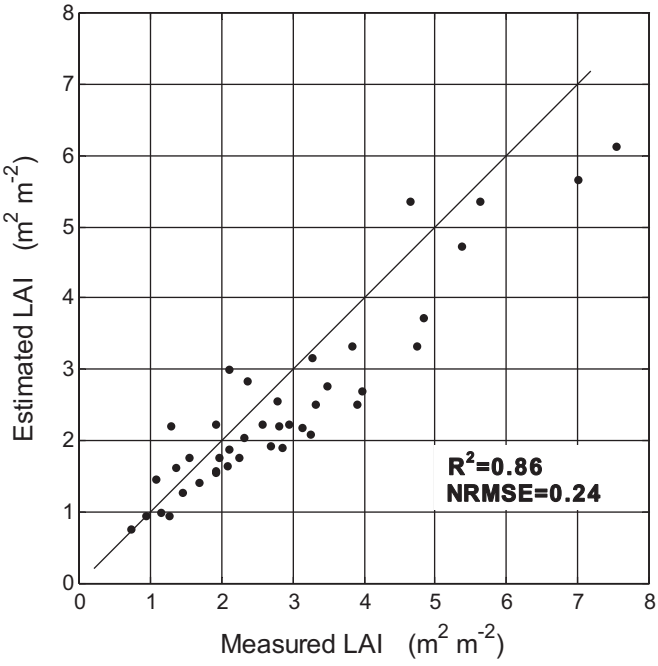

Fig. 8. Estimated versus measured LAI in Majella National Park, Italy, using the PROSAIL canopy reflectance model and the minimum RMSE criterion in the LUT search (n = 41).

Table 6
R^2, RMSE and normalized RMSE (nRMSE) between measured and estimated LAI (n = 41) from PROSAIL inversion. The standard LUT solution is indicated as "best fitting spectra". The LAI was also retrieved considering the mean of first 10 and 100 solutions.

No. of solutions	LAI (m^2 m^{-2})		
	R^2	RMSE	nRMSE
Best fitting spectra	0.86	0.70	0.24
First 10	0.89	0.63	0.22
First 100	0.85	0.62	0.22

Table 7
R^2, RMSE and normalized RMSE between measured and estimated LAI (n = 41) from PROSAIL inversion relating to the two spectral subsets.

Spectral sampling set	Statistical parameter	LAI (m^2 m^{-2})		
		R^2	RMSE	nRMSE
Using all wavelengths	Best fitting spectra	0.86	0.89	0.70
(n (λ) = 126)	Mean of 10	0.63	0.24	0.22
Subset I (n (λ) = 12)	Best fitting spectra	0.83	0.80	0.27
(based on literature)	Mean of 10	0.85	0.74	0.25
Subset II (n (λ) = 107)	Best fitting spectra	0.80	0.73	0.25
(based on AAE)	Mean of 10	0.91	0.53	0.18

Compared with the narrow band NDVI-like, the narrow band SAVI2-like gave somewhat higher R^2 (and lower normalized RMSE) values for LAI. This result is in agreement with findings of Broge and Leblanc (2001), who found SAVI2 to be an optimal vegetation index for LAI estimation as this index reduces the impact of soil background effects. Even though the vegetation indices gave satisfactory results in our research, one can not overlook the three main disadvantages that limit the usefulness of (2-band) vegetation indices: (i) they consider only part of the available (hyperspectral) information, (ii) they are more noise-sensitive as compared to full-spectrum methods (Atzberger et al., 2010), and (iii) they rely on the availability of reference data sets for model calibration.

Compared with narrow band indices, the partial least squares regression could not further improve the results beside a slight increase in the R^2 between measured and retrieved LAI (Table 5). This was not expected as information is lost when only two wavelengths are selected from the total spectral information available in hyperspectral data for narrow band vegetation indices (Lee et al., 2004).

By selecting a subset of wavelengths known to be strongly related to vegetation parameters (subset I), the results of partial least squares regression only slightly improved, contrary to findings in the literature (Kubinyi, 1996; Davies, 2001; Cho et al., 2007). A possible explanation is that subset I still contained wavebands with higher noise levels. This view is supported by the fact that subset I also gave lower accuracies when inverting the RTM, compared to subset II (with all wavebands eliminated not well represented by the RTM).

To make sure that PROSAIL is well adapted for simulating the Mediterranean grassland spectra given the measured LAI and C_{ab} values, its performance was evaluated in forward mode before starting the RTM inversion. The results of forward modeling revealed that most spectra were well modeled. Deviances between measured and simulated spectra were relatively modest even for the worst cases. It confirmed that with the ground measured LAI and C_{ab} (varied by 15 percent around their recorded value) one is able to simulate the observed spectra quite accurately. Thus it was concluded that the selected PROSAIL radiative transfer model can be employed for analyzing our Mediterranean grassland targets.

Concerning the inversion of physical models, Combal et al. (2003) and Meroni et al. (2004) have shown that utilizing prior information is an efficient way of solving the ill-posed problem and improving the accuracy of the estimated canopy variables. In the case of spatialized (remote sensing) data, Atzberger (2004) and Atzberger and Richter (2009, 2011) showed that for mono-species canopies the intercorrelation between spectral bands of neighboring pixel can be used to regularize the ill-posed inverse problem. However, the regularization of the inverse problem was beyond the scope of this study. We simply used the approximate maximum and minimum values from the field measurements for the three parameters *LAI*, C_{ab} and *ALA* as prior information for building the LUT and literature values for the remaining parameters. In this way, we increased the sampling density and constrained the estimated grass biophysical characteristics into reasonable ranges. However, the LUT should probably be adapted

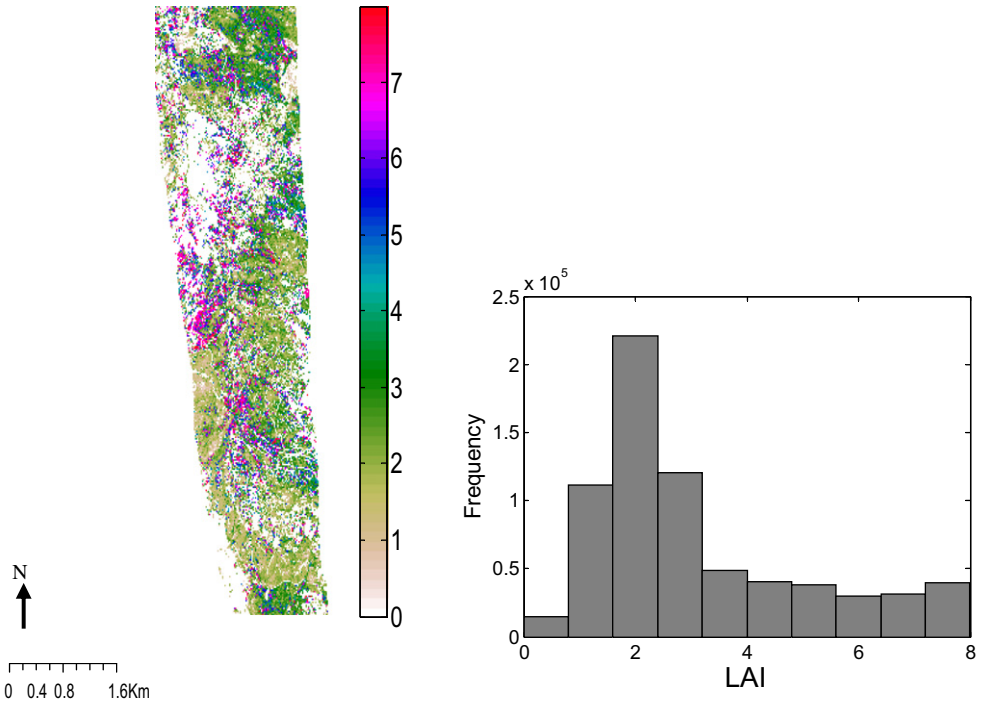

Fig. 9. Map (left) and frequency distribution (right) of PROSAIL derived LAI ($m^2\ m^{-2}$) for a subset area of Majella National Park, Italy, using the spectral subset II, mean of 10 (white areas on the map means not grassland).

when used in a study area with strongly different soil optical properties, as a local soil data base was used for constructing the LUT.

Albeit successful, the imposed upper/lower boundaries in the LUT had as a logical consequence that estimated parameters could not go beyond the imposed bounds. This contradicts somewhat the physical approach as the prior information has an overwhelming influence (Baret and Buis, 2008). On the other hand, this is what one expects in the case of an ill-posed inverse problem, which may lead to solutions far away from the true parameter combination. To avoid the solution reaching fixed boundaries one could instead use a modified cost function in the LUT search where the prior info is included directly in the calculation of the error surface (e.g., Combal et al., 2002; Houborg and Boegh, 2008; le Maire et al., 2008; Haboudane et al., 2008; Jacquemoud et al., 2009). Such a modified cost-function takes explicitly into account the expected mean value of a model parameter and the uncertainty of the provided prior info. A clear advantage of such an approach is that the influence of the prior info is much smoother.

In the present study, we also did not evaluate the possible benefits of regularization efforts published recently. Increased retrieval accuracies have, for example, been demonstrated by Lavergne et al. (2007) using the reflectance uncertainty matrix in the cost function. This would require, however, running the LUT inversion several times with boot-strap techniques to avoid that the measured and estimated biophysical variables become dependent.

The relationships between measured and estimated LAI were perceptibly improved when only wavelengths with low AAE (subset II and 10 best solutions) were used for model inversion. The result is in agreement with work of Meroni et al. (2004), Fang and Liang (2005), and Schlerf and Atzberger (2006). They demonstrated that, when inverting radiative transfer models, the selection of a few wavebands may give better results than those achieved using the full spectral resolution. No improvements could be found when using the spectral subset I, described in the literature as being 'optimum' for vegetation studies, probably because some of its wavebands are not well represented by PROSAIL.

6. Conclusion

The results of the study demonstrate that grass canopy LAI can be estimated through the inversion of a radiative transfer model with accuracies comparable to (or even better than) those of statistical approaches. In contrast to statistical approaches, ground-measured biophysical data may be almost entirely used for validating the retrieved model parameters (and for setting the LUT ranges) and are not used to calibrate the model (except the soil reflectance spectra that has to be input into the radiative transfer model). Once an appropriate LUT has been built, it can in principle be applied to different remote sensing data acquired over similar vegetation (and soil) types, thereby overcoming the main limitation of statistical models, which are known to be highly site- and sensor-specific. For example, in a previous study by Darvishzadeh et al. (2008a), a look up table approach was established and validated based on field spectra and the ground LAI measurements. In the present paper that same LUT was applied to HyMap imagery without further modification of the details in the inversion procedure (range of parameters, number of solutions, etc.). Our results show that the inversion procedure was successfully transferred to a sensor that has different spectral settings and that is operating on a different spatial scale.

The present results indicate that radiative transfer models and remotely sensed hyperspectral imaging can be linked for mapping and assessing leaf area index in Mediterranean grasslands with high accuracy (nRMSE = 0.18; R^2 = 0.91). The proposed inversion procedure and band selection scheme are of interest for the remote sensing community working on improved inversion schemes in specific spectral regions and for different vegetation types. With the aid of recently and future launched spaceborne hyperspectral sensors, e.g., Hyperion and EnMap, global data sets will be available. Hence the application of the developed methods to other vegetation types with mixed species can be evaluated to prove its robustness for mapping important vegetation biophysical and biochemical properties.

Acknowledgements

We would like to acknowledge the assistance of the park management of Majella National Park, Italy, and in particular of Dr. Teodoro Andrisano. Special thanks go to Dr. Fabio Corsi, Dr. Sip van Wieren, Dr. Moses Cho and Dr. Istiak Sobhan for their assistance during the field campaign. Many thanks go to Mr. Willem Nieuwenhuis for helping with the IDL programming. Our appreciation also goes to Dr. Michal Daszykowski for his assistance in applying the TOMCAT toolbox and for his valuable comments. We would like to thank the anonymous reviewers for helpful suggestions and comments.

References

Atzberger, C., 2004. Object-based retrieval of biophysical canopy variables using artificial neural nets and radiative transfer models. Remote Sensing of Environment 93 (1–2), 53–67.

Atzberger, C., Richter, K., 2009. Geostatistical regularization of inverse models for the retrieval of vegetation biophysical variables. SPIE Europe Remote Sensing, Berlin, Germany.

Atzberger, C., Guerif, M., Baret, F., Werner, W., 2010. Comparative assessment of three chemometric techniques for the spectroradiometric assessment of canopy chlorophyll content in winter wheat. Computers and Electronics in Agriculture 73, 165–173.

Atzberger, C., 2010. Inverting the PROSAIL canopy reflectance model using neural nets trained on streamlined databases. Journal of Spectral Imaging 1 (a2 (2010)), doi: 10.1255/jse.2010.ax.

Atzberger, C., Richter, K., 2011. Spatially-constraint inversion of radiative transfer models for improved LAI mapping from future Sentinel-2 imagery. Remote Sensing of Environment, accepted.

Atzberger, C., Jarmer, T., Schlerf, M., Kötz, B., Werner, W., 2003. Retrieval of wheat bio-physical attributes from hyperspectral data and SAILH + PROSPECT radiative transfer model. In: Habermeyer, M., Müller, A., Holzwarth, S. (Eds.), 3rd EARSeL Workshop on Imaging Spectroscopy. Herrsching, Germany, 13-16 May 2003, pp. 473-482.

Bacour, C., Baret, F., Beal, D., Weiss, M., Pavageau, K., 2006. Neural network estimation of LAI, fAPAR, fCover and LAIxC_{ab} from top of canopy MERIS reflectance data: principles and validation. Remote Sensing of Environment 105 (4), 313–325.

Bemigisha, J., 2008. Spectral and human sensors: hyperspectral remote sensing and participatory GIS for mapping livestock grazing intensity and vegetation in transhumant Mediterranean conservation areas. Ph.D. Thesis, Wageningen University.

Baret, F., Buis, S., 2008. Estimating canopy characteristics from remote sensing observations, Review of methods and associated problems. In: Liang (Ed.), Advances in land remote sensing system, modeling, inversion and application, e-book. Berlin, Springer.

Baret, F., Champion, I., Guyot, G., Podaire, A., 1987. Monitoring wheat canopies with a high spectral resolution radiometer. Remote Sensing of Environment 22 (3), 367–378.

Baret, F., Guyot, G., 1991. Potentials and limits of vegetation indices for LAI and APAR assessment. Remote Sensing of Environment 35 (2–3), 161–173.

Bateson, C.A., Asner, G.P., Wessman, C.A., 2000. Endmember bundles: a new approach to incorporating endmember variability into spectral mixture analysis. Geoscience and Remote Sensing IEEE Transactions 38 (2), 1083–1094.

Broge, N.H., Leblanc, E., 2001. Comparing prediction power and stability of broadband and hyperspectral vegetation indices for estimation of green leaf area index and canopy chlorophyll density. Remote Sensing of Environment 76 (2), 156–172.

Brown, L., Chen, J.M., Leblanc, S.G., Cihlar, J., 2000. A shortwave infrared modification to the simple ratio for LAI retrieval in boreal forests: an image and model analysis. Remote Sensing of Environment 71 (1), 16–25.

Campbell, R.J., Nobley, K.N., Marini, R.P., Pfeiffer, D.G., 1990. Growing conditions alter the relationship between SPAD-501 values and apple leaf chlorophyll. HortScience 25, 330–331.

Carter, G.A., 1994. Ratios of leaf reflectances in narrow wavebands as indicators of plant stress. International Journal of Remote Sensing 15 (3), 697–703.

Chaurasia, S., Dadhwal, V.K., 2004. Comparison of principal component inversion with VI-empirical approach for LAI estimation using simulated reflectance data. International Journal Remote Sensing 25 (14), 2881–2887.

Chen, J.M., Rich, P.M., Gower, S.T., Norman, J.M., Plummer, S., 1997. Leaf area index of boreal forests: theory, techniques, and measurements. Journal of Geophysical Research 102 (D24), 29429–29443.

Cho, M.A., 2007. Hyperspectral remote sensing of biochemical and biophysical parameters: the derivative red-edge "double-peak" feature: a nuisance or an opportunity? Ph.D. Thesis, Wageningen University.

Cho, M.A., Skidmore, A.K., 2006. A new technique for extracting the red edge position from hyperspectral data: The linear extrapolation method. Remote Sensing of Environment 101 (2), 181–193.

Cho, M.A., Skidmore, A., Corsi, F., van Wieren, S.E., Sobhan, I., 2007. Estimation of green grass/herb biomass from airborne hyperspectral imagery using spectral indices and partial least squares regression. International Journal of Applied Earth Observation and Geoinformation 9 (2007–4), 375–391.

Cho, M.A., Skidmore, A., Atzberger, C., 2008. Towards red - edge positions less sensitive to canopy biophysical parameters for leaf chlorophyll estimation using properties optique spectrales des feuilles PROSPECT and scattering by arbitrarily inclined leaves SAILH simulated data. International Journal of Remote Sensing 29 (8), 2241–2255.

Cimini, N., 2005. Parco nazionale della majella. Park Corporation, Programming and Planning Office.

Clevers, J.G.P.W., Verhoef, W., 1991. Modelling and synergetic use of optical and microwave remote sensing. Report 2: LAI estimation from canopy reflectance and WDVI: a sensitivity analysis with the SAIL model. BCRS Report 90-39.

Cohen, W.B., Goward, S.N., 2004. Landsat's role in ecological application of remote sensing. BioScience 54 (6), 535–545.

Colombo, R., Bellingeri, D., Fasolini, D., Marino, C.M., 2003. Retrieval of leaf area index in different vegetation types using high resolution satellite data. Remote Sensing of Environment 86 (1), 120–131.

Combal, B., Baret, F., Weiss, M., 2002. Improving canopy variables estimation from remote sensing data by exploiting ancillary information. Case study on sugar beet canopies. Agronomie 22 (2), 205–215.

Combal, B., Baret, F., Weiss, M., Trubuil, A., Mace, D., Pragnere, A., Myneni, R., Knyazikhin, Y., Wang, L., 2003. Retrieval of canopy biophysical variables from bidirectional reflectance. using prior information to solve the ill-posed inverse problem. Remote Sensing of Environment 84 (1), 1–15.

Curran, P.J., 1989. Remote sensing of foliar chemistry. Remote Sensing of Environment 30 (3), 271–278.

Danson, F.M., Rowland, C.S., Baret, F., 2003. Training a neural network with a canopy reflectance model to estimate crop leaf area index. International Journal of Remote Sensing 24 (23), 4891–4905.

Darvishzadeh, R., Atzberger, C., Skidmore, A., Abkar, A.A., 2009. Leaf area index derivation from hyperspectral vegetation indices and the red edge position. International Journal of Remote Sensing 30 (23), 6199–6218.

Darvishzadeh, R., Skidmore, A., Schlerf, M., Atzberger, C., 2008a. Inversion of a radiative transfer model for estimating vegetation LAI and chlorophyll in a heterogeneous grassland. Remote Sensing of Environment 112 (5), 2592–2604.

Darvishzadeh, R., Skidmore, A., Schlerf, M., Atzberger, C., Corsi, F., Cho, M.A., 2008b. LAI and chlorophyll estimated for a heterogeneous grassland using hyperspectral measurements. ISPRS Journal of Photogrammetry and Remote Sensing 63 (4), 409–426.

Daszykowski, M., Serneels, S., Kaczmarek, K., Van Espen, P., Croux, C., Walczak, B., 2007. TOMCAT: a MATLAB toolbox for multivariate calibration techniques. Chemometrics and Intelligent Laboratory Systems 85 (2), 269–277.

Davies, A.M.C., 2001. Uncertainty testing in PLS regression. Spectroscopy Europe 13 (2), 16–19.

Disney, M., Lewis, P., Saich, P., 2006. 3D modelling of forest canopy structure for remote sensing simulations in the optical and microwave domains. Remote Sensing of Environment 100 (1), 114–132.

Ehsani, M.R., Upadhyaya, S.K., Slaughter, D., Shafii, S., Pelletier, M., 1999. A NIR technique for rapid determination of soil mineral nitrogen. Precision Agriculture 1 (2), 217–234.

Fang, H., Liang, S., 2005. A hybrid inversion method for mapping leaf area index from MODIS data: experiments and application to broadleaf and needleleaf canopies. Remote Sensing of Environment 94 (3), 405–424.

Farifteh, J., van der Meer, F., Atzberger, C., Carranza, E.J.M., 2007. Quantitative analysis of salt-affected soil reflectance spectra: a comparison of two adaptive methods (PLSR and ANN). Remote Sensing of Environment 110 (1), 59–78.

Fava, F., Colombo, R., Bocchi, S., Meroni, M., Sitzia, M., Fois, N., Zucca, C., 2009. Identification of hyperspectral vegetation indices for Mediterranean pasture characterization. International Journal of Applied Earth Observation and Geoinformation 11 (4), 233–243.

Fisher, P., 1997. The pixel: a snare and a delusion. International Journal of Remote Sensing 18 (3), 679–685.

Fourty, T., Baret, F., 1997. Vegetation water and dry matter contents estimated from top-of-the-atmosphere reflectance data: a simulation study. Remote Sensing of Environment 61 (1), 34–45.

Fourty, T., Baret, F., Jacquemoud, S., Schmuck, G., Verdebout, J., 1996. Leaf optical properties with explicit description of its biochemical composition: direct and inverse problems. Remote Sensing of Environment 56 (2), 104–117.

Geladi, P., Kowalski, B.R., 1986. Partial least-squares regression: a tutorial. Analytica Chimica Acta 185, 1–17.

Gemmell, F., Varjo, J., Strandstrom, M., Kuusk, A., 2002. Comparison of measured boreal forest characteristics with estimates from TM data and limited ancillary information using reflectance model inversion. Remote Sensing of Environment 81 (2–3), 365–377.

Gitelson, A.A., Merzlyak, M.N., 1997. Remote estimation of chlorophyll content in higher plant leaves. International Journal of Remote Sensing 18 (12), 2691–2697.

Goel, N.S., 1989. Inversion of canopy reflectance models for estimation of biophysical parameters from reflectance data. In: Asrar, G. (Ed.), Theory and applications of optical remote sensing. Wiley & Sons, New York, pp. 205–251.

Guyot, G., Baret, F., 1988. Utilisation de la haute résolution spectrale pour suivre l'état des couverts végétaux. In: Guyenne, T.D., Hunt, J.J. (Eds.), Proc. 4th

international colloquium on spectral signatures of objects in Remote Sensing. ESA SP-287, Aussois, France, 18-22 January 1988, 279-286.
Haboudane, D., Miller, J.R., Pattey, E., Zarco-Tejada, P.J., Strachan, I.B., 2004. Hyperspectral vegetation indices and novel algorithms for predicting green LAI of crop canopies: modeling and validation in the context of precision agriculture. Remote Sensing of Environment 90 (3), 337–352.
Haboudane, D., Miller, J.R., Tremblay, N., Zarco-Tejada, P.J., Dextraze, L., 2002. Integrated narrow-band vegetation indices for prediction of crop chlorophyll content for application to precision agriculture. Remote Sensing of Environment 81 (2–3), 416–426.
Haboudane, D., Tremblay, N., Miller, J.R., Vigneault, P., 2008. Remote Estimation of Crop Chlorophyll Content Using Spectral Indices Derived From Hyperspectral Data. Geoscience and Remote Sensing IEEE Transactions 46 (2), 423–437.
Hansen, P.M., Schjoerring, J.K., 2003. Reflectance measurement of canopy biomass and nitrogen status in wheat crops using normalized difference vegetation indices and partial least squares regression. Remote Sensing of Environment 86 (4), 542–553.
Horler, D.N.H., Dockray, M., Barber, J., 1983. The red edge of plant leaf reflectance. International Journal of Remote Sensing 4 (2), 273–288.
Houborg, R., Soegaard, H., Boegh, E., 2007. Combining vegetation index and model inversion methods for the extraction of key vegetation biophysical parameters using Terra and Aqua MODIS reflectance data. Remote Sensing of Environment 106 (1), 39–58.
Houborg, R., Boegh, E., 2008. Mapping leaf chlorophyll and leaf area index using inverse and forward canopy reflectance modeling and SPOT reflectance data. Remote Sensing of Environment 112 (1), 186–202.
Houborg, R., Anderson, M., et al., 2009. Utility of an image-based canopy reflectance modeling tool for remote estimation of LAI and leaf chlorophyll content at the field scale. Remote Sensing of Environment 113 (1), 259–274.
Jacquemoud, S., Bacour, C., Poilve, H., Frangi, J.-P., 2000. Comparison of four radiative transfer models to simulate plant canopies reflectance: direct and inverse mode. Remote Sensing of Environment 74 (3), 471–481.
Jacquemoud, S., Baret, F., 1990. PROSPECT: a model of leaf optical properties spectra. Remote Sensing of Environment 34 (2), 75–91.
Jacquemoud, S., Baret, F., Hanocq, J.F., 1992. Modeling spectral and bidirectional soil reflectance. Remote Sensing of Environment 41 (2–3), 123–132.
Jacquemoud, S., Ustin, S.L., Verdebout, J., Schmuck, G., Andreoli, G., Hosgood, B., 1996. Estimating leaf biochemistry using the PROSPECT leaf optical properties model. Remote Sensing of Environment 56 (3), 194–202.
Jacquemoud, S., Verhoef, W., Baret, F., Bacour, C., Zarco-Tejada, P.J., Asner, G.P., François, C., Ustin, S.L., 2009. PROSPECT + SAIL models: a review of use for vegetation characterization. Remote Sensing of Environment 113 (Supplement 1), S56–S66.
Knyazikhin, Y., Glassy, J., Privette, J.L., Tian, Y., Lotsch, A., Zhang, Y., Wang, Y., Morisette, J.T., Votava, P., Myneni, R.B., Nemani, R.R., Running, S.W., 1999. MODIS Leaf Area Index (LAI) and Fraction of Photosynthetically Active Radiation Absorbed by Vegetation (FPAR) Product (MOD15) Algorithm, Theoretical Basis Document, NASA Goddard Space Flight Center, Greenbelt, MD 20771, USA.
Kooistra, L., Salas, E.A.L., Clevers, J.G.P.W., Wehrens, R., Leuven, R.S.E.W., Nienhuis, P.H., Buydens, L.M.C., 2004. Exploring field vegetation reflectance as an indicator of soil contamination in river floodplains. Environmental Pollution 127 (2), 281–290.
Kubinyi, H., 1996. Evolutionary variable selection in regression and PLS analyses. Journal of Chemometrics 10 (2), 119–133.
Kuusk, A., 1991. The hot-spot effect in plant canopy reflectance. In: Myneni, R.B., Ross, J. (Eds.), Photon-vegetation interactions. Springer-Verlag, New York, pp. 139–159.
Lavergne, T., Kaminski, T., Pinty, B., Taberner, M., Gobron, N., Verstraete, M.M., Vossbeck, M., Widlowski, J.-L., Giering, R., 2007. Application to MISR land products of an RPV model inversion package using adjoint and Hessian codes. Remote Sensing of Environment 107 (1–2), 362–375.
Lee, K.-S., Cohen, W.B., Kennedy, R.E., Maiersperger, T.K., Gower, S.T., 2004. Hyperspectral versus multispectral data for estimating leaf area index in four different biomes. Remote Sensing of Environment 91 (3–4), 508–520.
le Maire, G., Francois, C., Dufrene, E., 2004. Towards universal broad leaf chlorophyll indices using PROSPECT simulated database and hyperspectral reflectance measurements. Remote Sensing of Environment 89 (1), 1–28.
le Maire, François, Soudani, Berveiller, Pontailler, Bréda, Genet, Davi, Dufrêne, 2008. Calibration and validation of hyperspectral indices for the estimation of broadleaved forest leaf chlorophyll content, leaf mass per area, leaf area index and leaf canopy biomass. Remote Sensing of Environment 112 (10), 3846–3864.
Liang, S., 2004. Quantitative remote sensing of land surfaces. Wiley Praxis Series in Remote Sensing. Wiley & Sons, Hoboken.
OR, L.I.-C., 1992. LAI-2000 plant canopy analyzer instruction manual. LICOR Inc., Lincoln. NE, USA.
Major, D.J., Baret, F., Guyot, G., 1990. A ratio vegetation index adjusted for soil brightness. International Journal of Remote Sensing 11 (5), 727–740.
Markwell, J., Osterman, J.C., Mitchell, J.L., 1995. Calibration of Minolta SPAD-502 leaf chlorophyll meter. Photosynthetic Research 46 (3), 467–472.
Meroni, M., Colombo, R., Panigada, C., 2004. Inversion of a radiative transfer model with hyperspectral observations for LAI mapping in poplar plantations. Remote Sensing of Environment 92 (2), 195–206.
Minolta, 2003. Chlorophyll meter SPAD-502. Instruction Manual, Minolta Camera BeNeLux BV. Maarssen, The Netherlands.
Mutanga, O., Skidmore, A.K., 2004. Narrow band vegetation indices overcome the saturation problem in biomass estimation. International Journal of Remote Sensing 25 (19), 3999–4014.
Nemani, R.R., Pierce, L.L., Running, S.W., Band, L.E., 1993. Forest ecosystem processes at the watershed scale: sensitivity to remotely sensed leaf area index estimates. International Journal of Remote Sensing 14 (13), 2519–2534.
Pu, R., Gong, P., Biging, G.S., Larrieu, M.R., 2003. Extraction of red edge optical parameters from Hyperion data for estimation of forest leaf area index. IEEE Transactions on Geoscience and Remote Sensing 41 (4), 916–921.
Richter, K., Atzberger, C., Vuolo, F., Weihs, P., d'Urso, G., 2009. Experimental assessment of the Sentinel-2 band setting for RTM-based LAI retrieval of sugar beet and maize. Candian Journal of Remote Sensing 35 (3), 230–247.
Röder, A., Kuemmerle, T., Hill, J., Papanastasis, V.P., Tsiourlis, G.M., 2007. Adaptation of a grazing gradient concept to heterogeneous Mediterranean rangelands using cost surface modelling. Ecological Modelling 204 (3–4), 387–398.
Rouse, J.W., Haas, R.H., Schell, J.A., Deering, D.W., Harlan, J.C., 1974. Monitoring the vernal advancement of retrogradation of natural vegetation. NASA/GSFC, type III Final report. Greenbelt, MD.
Schaepman, M.E., Ustin, S.L., Plaza, A.J., Painter, T.H., Verrelst, J., Liang, S., 2009. Earth system science related imaging spectroscopy-An assessment. Remote Sensing of Environment 113 (Suppl. 1), S123–S137.
Schiefer, S., Hostert, P., Damm, A., 2006. Correcting brightness gradients in hyperspectral data from urban areas. Remote Sensing of Environment 101 (1), 25–37.
Schlerf, M., Atzberger, C., 2006. Inversion of a forest reflectance model to estimate structural canopy variables from hyperspectral remote sensing data. Remote Sensing of Environment 100 (3), 281–294.
Schlerf, M., Atzberger, C., Hill, J., 2005. Remote sensing of forest biophysical variables using HyMap imaging spectrometer data. Remote Sensing of Environment 95 (2), 177–194.
Schlerf, M., Atzberger, C., Udelhoven, T., Jarmer, T., Mader, S., Werner, W., Hill, J., 2003. Spectrometric estimation of leaf pigments in Norway spruce needles using band-depth analysis, partial least-square regression and inversion of a conifer leaf model. In: Habermeyer, M., Müller, A., Holzwarth, S. (Eds.), Proc. 3rd EARSeL workshop on imaging spectroscopy. Herrsching, Germany, 13-16 May 2003, 559-568.
Schlerf, M., Atzberger, C., Hill, J., Buddenbaum, H., Werner, W., Schueler, G., 2010. Retrieval of chlorophyll and nitrogen in Norway spruce (Picea abies L. Karst) using imaging spectroscopy. International Journal of Applied Earth Observation and Geoinformation 12, 17–26.
Stuckens, J., Somers, B., Delalieux, S., Verstraeten, W.W., Coppin, P., 2009. The impact of common assumptions on canopy radiative transfer simulations: A case study in Citrus orchards. Journal of Quantitative Spectroscopy and Radiative Transfer 110 (1–2), 1–21.
Tang, S., Chen, J.M., Zhu, Q., Li, X., Chen, M., Sun, R., Zhou, Y., Deng, F., Xie, D., 2006. LAI inversion algorithm based on directional reflectance kernels. Journal of Environmental Management 85 (3), 638–648.
Thenkabail, P.S., Enclona, E.A., Ashton, M.S., Legg, C., De Dieu, M.J., 2004. Hyperion, IKONOS, ALI, and ETM + sensors in the study of African rainforests. Remote Sensing of Environment 90 (1), 23–43.
Thenkabail, P.S., Smith, R.B., De Pauw, E., 2000. Hyperspectral vegetation indices and their relationships with agricultural crop characteristics. Remote Sensing of Environment 71 (2), 158–182.
Turner, D.P., Cohen, W.B., Kennedy, R.E., Fassnacht, K.S., Briggs, J.M., 1999. Relationships between leaf area index and Landsat TM spectral vegetation indices across three temperate zone sites. Remote Sensing of Environment 70 (1), 52–68.
Verhoef, W., 1984. Light scattering by leaf layers with application to canopy reflectance modeling: the SAIL model. Remote Sensing of Environment 16 (2), 125–141.
Verhoef, W., 1985. Earth observation modeling based on layer scattering matrices. Remote Sensing of Environment 17 (2), 165–178.
Vohland, M., Jarmer, T., 2008. Estimating structural and biochemical parameters for grassland from spectroradiometer data by radiative transfer modelling (PROSPECT + SAIL). International Journal of Remote Sensing 29 (1), 191–209.
Weiss, M., Baret, F., 1999. Evaluation of canopy biophysical variable retrieval performances from the accumulation of large swath satellite data. Remote Sensing of Environment 70 (3), 293–306.
Weiss, M., Baret, F., Myneni, R.B., Pragnère, A., Knyazikhin, Y., 2000. Investigation of a model inversion technique to estimate canopy biophysical variables from spectral and directional reflectance data. Agronomie 20, 3–22.
Welles, J.M., Norman, J.M., 1991. Instrument for indirect measurement of canopy architecture. Agronomy Journal 83 (5), 818–825.
Wessman, C.A., Aber, J.D., Peterson, D.L., Melillo, J.M., 1988. Remote sensing of canopy chemistry and nitrogen cycling in temperate forest ecosystems. Nature 335, 154–156.
White, J.D., Running, S.W., Nemani, R., Keane, R.E., Ryan, K.C., 1997. Measurement and remote sensing of LAI in rocky mountain montane ecosystems. Canadian Journal of Forest Research 27 (11), 1714–1727.
Zarco-Tejada, P.J., Miller, J.R., Harron, J., Hu, B., Noland, T.L., Goel, N., Mohammed, G.H., Sampson, P., 2004. Needle chlorophyll content estimation through model inversion using hyperspectral data from boreal conifer forest canopies. Remote Sensing of Environment 89 (2), 189–199.